

DCoM: Competence-Driven Adaptive Active Learning

Inbal Mishal[†], Daphna Weinshall[†]

School of Computer Science & Engineering[†]
The Hebrew University of Jerusalem
Jerusalem 91904, Israel
{inbal.mishal,daphna}@mail.huji.ac.il

Abstract

Deep Active Learning techniques can be effective in reducing annotation costs for training deep models. However, their effectiveness in low- and high-budget scenarios seems to require different strategies, and achieving optimal results across varying budget scenarios remains a challenge. In this study, we introduce Dynamic Coverage & Margin mix (*DCoM*), a novel active learning approach designed to bridge this gap. Unlike existing strategies, *DCoM* dynamically adjusts its strategy, while taking into account the competence of the current model. Through theoretical analysis and empirical evaluations on diverse datasets, including challenging computer vision tasks, we demonstrate *DCoM*'s ability to overcome the cold start problem and consistently improve results across different budgetary constraints. Thus *DCoM* achieves state-of-the-art performance in both low- and high-budget regimes.

1 Introduction

Deep Learning (DL) algorithms require large amounts of data to achieve optimal results. In some situations, there is an abundance of unlabeled data but limited capacity to label it. In fields such as medical imaging, an invaluable resource — doctors themselves — serves as a costly oracle.

Active learning (AL) algorithms aim to address this challenge by reducing the labeling burden and enhancing its effectiveness (see illustration in Fig. 1). Unlike traditional supervised learning frameworks, AL can influence the construction of the labeled set, potentially by leveraging knowledge about the current learner. Accordingly, the initial goal of AL is to select q examples to be annotated, where q represents the number of examples that can be sent to the oracle. AL has already demonstrated tangible contributions across various domains such as computer vision tasks (e.g. Yuan et al. 2023), NLP (e.g. Siddhant and Lipton 2018; Kaseb and Farouk 2023) and medical imaging (e.g. El-Hasnony et al. 2022). These examples highlight the importance of advancing AL to achieve even greater impact.

The choice of an active learning (AL) strategy depends on both the learner's inductive biases and the nature of the problem. Recent research indicates that the optimal AL strategy varies with the budget size, where the budget refers to the size of the training set. For larger budgets, uncertainty and diversity sampling methods are most effective, while for smaller budgets, strategies focused on typicality and diversity

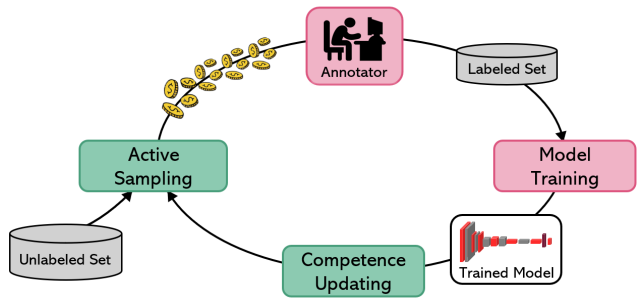


Figure 1: Illustration of the AL iterative process: *DCoM* introduces an additional step to estimate the current learner's competence, which is then utilized during the active sampling phase.

are more suitable. However, no single AL strategy is universally optimal across all budget levels. Our study addresses this challenge by dynamically selecting the best examples based on the learner's current state and the available budget.

Recent research, as briefly reviewed below, often categorizes active sampling methods based on budget regimes. In contrast, our study takes a different approach by emphasizing the need to adapt sample selection methods according to the learner's competence. We aim to develop a single algorithm that dynamically adjusts its sampling strategy in response to the learner's evolving abilities. This shift from a budget-focused to a competence-driven approach represents a significant advancement in active learning research, allowing for a more adaptive strategy that optimizes performance based on measurable learner's capabilities.

In this work, we introduce a novel method called Dynamic Coverage & Margin Mix (*DCoM*), which dynamically adjusts its selection strategy by minimizing a new loss function that incorporates a measure of competence. We start by exploring a simplified theoretical framework (Section 2), where we integrate a typicality test with an uncertainty test based on the budget and a notion of coverage. Building on the insights from this analysis, we introduce *DCoM* (Section 3), which combines these elements to provide a flexible solution for any budget. Thus, *DCoM* selects the most appropriate examples suited to the current budget. We validate *DCoM* through an extensive empirical study using various vision datasets (Section 4), demonstrating that *DCoM* consistently achieves superior performance across all budget ranges.

Relation to prior art. Over the past years, active learning has been an active area of research (Wang et al. 2023; Settles 2009; Cohn, Ghahramani, and Jordan 1996; Tharwat and Schenck 2023; Xie et al. 2023; Schmidt et al. 2024). The realm of Active Learning (AL) is segmented into three problem settings: membership query synthesis, stream-based selective sampling, and pool-based active learning (Settles 2009). Much of the recent AL work follows the pool-based setting, where samples are selected from a large pool of unlabeled data and annotations are obtained from an oracle. In this setting, AL algorithms operate within a given budget (b), selecting a subset of unlabeled examples to send to an oracle for labeling. This selection process aims to identify examples that will maximize the model’s performance. This process may be repeated iteratively, gradually increasing budget b .

In discussions of pool-based AL, two key characteristics that play a crucial role during the active sampling process are *uncertainty* and *diversity*. Some AL algorithms focus solely on uncertainty sampling (Lewis and Gale 1994; Shannon 1948; Cho et al. 2023; Zhao et al. 2021; Houlsby et al. 2011; Gissin and Shalev-Shwartz 2019; Ranganathan et al. 2017; Woo 2022; Gal, Islam, and Ghahramani 2017; Parvaneh et al. 2022; Jung, Kim, and Lee 2023), while others prioritize diversity sampling (Sener and Savarese 2018; Hu, Mac Namee, and Delany 2010; Yehuda et al. 2022; Hacohen, Dekel, and Weinshall 2022). Other algorithms combine both uncertainty and diversity in their approaches (Yang et al. 2015; Chen et al. 2024; Wen, Pizarro, and Williams 2023; Kirsch, Van Amersfoort, and Gal 2019; Chowdhury, Hamerly, and McGarrity 2024; Ash et al. 2019; Kim et al. 2021).

Over time, the cold start problem has emerged, highlighting the difficulties faced by AL algorithms when operating with a small budget. It seems that *uncertainty* and *diversity* are ill-suited to address this challenge. Accordingly, Chen et al. (2024) describe the cold start problem as a combination of two issues: unbalanced sampling across different classes (which relates to diversity), and unbalanced sampling within each class, where uncertain examples are favored over certain ones at the outset.

In low-budget scenarios, typical examples often offer the highest benefits for training the model (Hacohen, Dekel, and Weinshall 2022; Yehuda et al. 2022; Chen et al. 2024). This implies that in such contexts, AL algorithms should aim to maximize both certainty and diversity. Conversely, in high-budget scenarios, the emphasis shifts towards maximizing uncertainty while maintaining diversity. While (Hacohen and Weinshall 2024) proposes a method to select the most suitable approach for the current state, the method involves the comparison of multiple active learning strategies at each state, rather than recommending a single universal approach.

Summary of contribution. (i) Expand a theoretical framework to analyze Active Learning (AL) strategies in embedding spaces. (ii) Introduce *DCoM*, a universal strategy that significantly outperforms previous methods in low and medium budget scenarios, and matches them in high budget scenarios. (iii) Initiate a transition from a budget-based discussion to the learner’s competence, while introducing coverage as a measure designed to predict competence.

2 Theoretical Framework

Let \mathbb{X} denote the input domain, \mathbb{Y} the target domain, and $\mathcal{L} : \mathbb{X} \rightarrow \mathbb{Y}$ the trained learner. Before seeing any labels, \mathcal{L} may be a random feasible hypothesis, or it may be initialized by either transfer learning or self training. Let b denote the size of the labeled training set, aka *budget*.

Active learning may involve a single step, or an iterative process with repeated active learning steps. In each AL step, the learner actively seeks labels by choosing a set of unlabeled points as a query set, to be labeled by an oracle/teacher. Subsequently, this set of labeled points is added to the learner’s supervised training set, and the learner is either retrained or fine-tuned.

As discussed in Section 1, it has been shown that different active learning strategies are suited for different budgets b . With a low budget b , strategies that do not rely on the outcome of the learner are most suitable. When b is high, it is beneficial to consider the confidence of the learner when choosing an effective query set. What makes a certain budget b high or low is left vague in previous work, as it depends on both the hypothesis space (or architecture) and the dataset.

To achieve an effective active learning protocol suitable for all learners, irrespective of budget, we aim to devise a universal objective function, whose minimization is used to select the query set. We begin by proposing to replace the notion of *budget* with the notion of *competence*, designed to track the generalization ability of \mathcal{L} when trained with budget b . The notion of competence, we hypothesize, is more universal and less dependent on the type of learner and specific dataset (see discussion in Section 2.3).

We then rephrase the intuition stated above (see Section 1) as follows: When the learner’s competence is low, the objective function should prioritize typicality and diversity of selected queries irrespective of the learner’s predictions. When the learner’s competence is high, its uncertainty in prediction should be given high priority.

More formally, let $\mathcal{O}(x)$ denote the desired objective function for query selection, where $x \in \mathbb{X}$ is unlabeled. Let $\mathcal{O}_{low}(x)$ and $\mathcal{O}_{high}(x)$ denote the objective functions suitable for a learner with low competence and high competence respectively. Let $S_{\mathcal{L}}$ denote a score, which captures the competence of learner \mathcal{L} . The proposed objective function can now be written as follows $\forall x \in \mathbb{X}$:

$$\mathcal{O}(x) = (1 - S_{\mathcal{L}}) \cdot \mathcal{O}_{low}(x) + S_{\mathcal{L}} \cdot \mathcal{O}_{high}(x) \quad (1)$$

After the introduction of necessary preliminaries in Section 2.1 we discuss in Section 2.2 the design of $\mathcal{O}_{low}(x)$. We begin with the point coverage framework introduced by Yehuda et al. (2022). This approach relies on self-supervised data representation, which is blind to the learner’s performance. We refine their analysis and obtain an improved generalization bound for the Nearest Neighbor classification model that depends on the local geometry of the data.

Next, in Section 2.3 we discuss our choice of $S_{\mathcal{L}}$, and connect it to the notion of budget discussed in previous work. Finally, we select $\mathcal{O}_{high}(x)$ to equal one minus the normalized lowest response between the two highest softmax outputs of \mathcal{L} at x , or *Margin*, as this is a common uncertainty measure.

2.1 Preliminaries

Notations. Let P denote the underlying probability distribution of data \mathbb{X} . Assume that a true labeling function $f : \mathbb{X} \rightarrow \mathbb{Y}$ exists. Let $\mathbb{U} \subseteq \mathbb{X}$ denote the unlabeled set of points, and $\mathbb{L} \subseteq \mathbb{X}$ the labeled set, such that $\mathbb{X} = \mathbb{U} \cup \mathbb{L}$. Here $|\mathbb{L}| = b \leq m$ is the annotation budget where $|\mathbb{X}| = m$.

Let $B_\delta(x) = \{x' \in \mathbb{X} : \|x' - x\|_2 \leq \delta\}$ denote a ball of radius δ centered at x . Let $C \equiv C(\mathbb{L}, \delta) = \bigcup_{x \in \mathbb{L}} B_\delta(x)$ denote the region covered by δ -balls centered at the labeled examples in \mathbb{L} . We call $C(\mathbb{L}, \delta)$ the *covered region*, where $P(C)$ denotes its probability. Let f^N denote the 1-NN classifier, and \mathcal{L} denote our current learner – a 1-NN classifier based on \mathbb{L} .

Definition 2.1. We say that a ball $B_\delta(x)$ is *pure* if $\forall x' \in B_\delta(x) : f(x') = f(x)$.

Definition 2.2. We define the *purity* of δ as

$$\pi(\delta) = P(\{x \in \mathbb{X} : B_\delta(x) \text{ is pure}\}).$$

Note that $\pi(\delta)$ is monotonically decreasing, as can be readily verified.

In (Yehuda et al. 2022) it is shown that the generalization error of the 1-NN classifier f^N is bounded as follows

$$\mathbb{E}[f^N(x) \neq f(x)] \leq (1 - P[C(\mathbb{L}, \delta)]) + (1 - \pi(\delta)). \quad (2)$$

Subsequently, an algorithm is proposed that minimizes the first term in (2) by maximizing the coverage probability $P[C(\mathbb{L}, \delta)]$, while ignoring the second term that is assumed to be fixed.

Below, we begin by refining the bound, focusing more closely on its second term ($1 - \pi(\delta)$). This is used in Section 3 to device an improved algorithm that minimizes simultaneously both terms of the refined error bound.

2.2 Refined error bound

Define the indicator random variable $I_\delta(x)$ as follows:

$$I_\delta(x) = \mathbb{1}_{\{x \in \mathbb{X} : B_\delta(x) \text{ is pure}\}}.$$

By definition,

$$\pi(\delta) = P(\{x \in \mathbb{X} : B_\delta(x) \text{ is pure}\}) = \mathbb{E}[I_\delta(x)].$$

Since the distribution of \mathbb{X} is not known apriori, we use the *empirical distribution* to approximate the expected value of this random variable. Thus, with labeled set $\mathbb{L} = \{x_i\}_{i=1}^b$

$$\begin{aligned} \hat{\pi}(\delta) &= \hat{\mathbb{E}}[\mathbb{1}_{\{x \in \mathbb{L} : B_\delta(x) \text{ is pure}\}}] = \frac{1}{b} \mathbb{E}\left[\sum_{i=1}^b \mathbb{1}_{\{B_\delta(x_i) \text{ is pure}\}}\right] \\ &= \frac{1}{b} \sum_{i=1}^b \mathbb{E}[\mathbb{1}_{\{B_\delta(x_i) \text{ is pure}\}}] = \frac{1}{b} \sum_{i=1}^b P[B_\delta(x_i) \text{ is pure}]. \end{aligned}$$

With this approximation

$$\begin{aligned} \mathbb{E}[f^N(x) \neq f(x)] &\leq \left[1 - P[C(\mathbb{L}, \delta)]\right] \\ &\quad + \left[1 - \frac{1}{b} \sum_{i=1}^b P[B_\delta(x_i) \text{ is pure}]\right] + \varepsilon. \end{aligned} \quad (3)$$

where $\varepsilon \xrightarrow[b \rightarrow \infty]{} 0$ bounds the error of the approximation $\hat{\pi}(\delta)$.

Note that the refined bound in (3) depends on the purity separately at each labeled point in \mathbb{L} . Next, we further refine this bound by allowing the fixed radius δ to be chosen individually, where δ_i denotes the radius of point $x_i \in \mathbb{L}$. Let $\Delta = [\delta_i]_{i=1}^b$ denote the list of individual radii corresponding to $\mathbb{L} = \{x_i\}_{i=1}^b$. The cover defined by Δ is $C(\mathbb{L}, \Delta) = \bigcup_{(x_i, \delta_i) \in \mathbb{L} \times \Delta} B_{\delta_i}(x_i)$.

With this choice, it is necessary to replace the 1-NN classifier with a suitable variant of nearest neighbor classification - the *normalized Nearest Neighbor* (1-nNN) classifier. In 1-nNN, distances to point $x_i \in \mathbb{L}$ are normalized by the corresponding δ_i , after which the nearest neighbor $f^N(x) = \operatorname{argmin}_{x_i \in \mathbb{L}} \frac{d(x, x_i)}{\delta_i}$ is computed. This transition preserves the original problem settings, and guarantees that if a labeled point $c \in \mathbb{L}$ assigns labels to other points, it also covers them (see Appendix B). Consequently, if a point x is mislabeled, there exists a $c \in \mathbb{L}$ that covers it, leading to a reduction in purity. The bound on the error in (3) becomes

$$\begin{aligned} \mathbb{E}[f^N(x) \neq f(x)] &\leq \left[1 - P[C(\mathbb{L}, \Delta)]\right] \\ &\quad + \left[1 - \frac{1}{b} \sum_{i=1}^b P[B_{\delta_i}(x_i) \text{ is pure}]\right] + \varepsilon. \end{aligned} \quad (4)$$

This bound describes a trade-off between probability coverage and purity, and guides the algorithm design in Section 3. Note that in (4), the cover $P[B_{\delta_i}(x_i) \text{ is pure}]$ is refined locally, using B_{δ_i} instead of B_δ .

2.3 Competence score $S_{\mathcal{L}}$

In order to obtain a useful competence score¹, which can be effectively used in objective function (1), we require that it satisfies the following conditions: (i) Lie in the range $[0, 1]$; (ii) Depend on the entire dataset; (iii) Monotonically increase with the competence of learner \mathcal{L} . In accordance, we propose to use a constrained Sigmoid function that depends on the probability of coverage:

$$S_{\mathcal{L}}(\mathbb{L}, \Delta) = \frac{1 + e^{-k(1-a)}}{1 + e^{-k(P[C(\mathbb{L}, \Delta)]-a)}} \quad (5)$$

This score follows the sigmoid curve, where a denotes its midpoint and k the steepness of the curve. In Appendix C, we analyze the choice of these parameters and its impact on the algorithm. Note that this score satisfies the conditions stated above for the nNN classifier: (i)-(ii), as it is a function in $[0, 1]$ that depends on $P[C(\mathbb{L}, \Delta)] = \frac{|C(\mathbb{L}, \Delta)|}{|\mathbb{X}|}$, while (iii) follows from the error bound (4).

Below, we demonstrate that $S_{\mathcal{L}}$ is monotonically increasing with the budget b , which supports the alignment of definition (5) with empirical evidence from prior work. Specifically, Hacohen, Dekel, and Weinshall (2022) showed both empirically and theoretically that the training budget $b = |\mathbb{L}|$ serves

¹When the labeled set \mathbb{L} is large, it may be possible to set aside a validation set to directly estimate the competence of learner \mathcal{L} , but this is not feasible when the labeled set \mathbb{L} is small.

as a valuable indicator for the relative suitability of $\mathcal{O}_{low}(x)$ and $\mathcal{O}_{high}(x)$, which are employed in (1). In our formulation, this relationship informs a trade-off represented by the score $S_{\mathcal{L}}(\mathbb{L}, \Delta)$ defined in (5). It remains to be shown that $S_{\mathcal{L}}(\mathbb{L}, \Delta)$ is indeed monotonically increasing with b .

Proposition. For two labeled sets \mathbb{L}, \mathbb{L}' , if $\mathbb{L} \subseteq \mathbb{L}'$ then $S_{\mathcal{L}}(\mathbb{L}, \Delta) \leq S_{\mathcal{L}}(\mathbb{L}', \Delta')$.

Proof. First, we note that

$$\begin{aligned} \mathbb{L} \subseteq \mathbb{L}' &\implies C(\mathbb{L}, \Delta) = \bigcup_{x_i \in \mathbb{L}} B_{\delta_i}(x_i) \\ &\subseteq \left(\bigcup_{x_i \in \mathbb{L}} B_{\delta_i}(x_i) \right) \cup \left(\bigcup_{x_i \in \mathbb{L}' \setminus \mathbb{L}} B_{\delta_i}(x_i) \right) \\ &= C(\mathbb{L}', \Delta') \end{aligned}$$

Since probability is monotonic, it follows that $P[C(\mathbb{L}, \Delta)] \leq P[C(\mathbb{L}', \Delta')]$. From (5), and by the definition of the logistic function using the provided parameters limits, $S_{\mathcal{L}}(\mathbb{L}, \Delta)$ is monotonically increasing in \mathbb{L} , which implies that $S_{\mathcal{L}}(\mathbb{L}, \Delta) \leq S_{\mathcal{L}}(\mathbb{L}', \Delta')$. \square

3 Our method: **DCoM**

The error bound presented in (4), derived in Section 2 by our theoretical analysis, highlights the trade-off between maximizing coverage $P[C(\mathbb{L}, \Delta)]$ and maintaining high purity $P[\bigcup_i \{B_{\delta_i}(x_i) \text{ is pure}\}]$ while seeking an optimal query set. The analysis also highlights the benefit of using a dynamic competence score to adjust the algorithm's objective function based on coverage. Below, we incorporate these principles into a new active learning strategy called **DCoM**, a unified active learning strategy designed for all budget scenarios. Notably, since (Yehuda et al. 2022) demonstrated that maximizing coverage is an NP-hard problem, we address this challenge with a greedy algorithm for query selection.

3.1 Framework and definitions

$\forall x \in \mathbb{X}$, let $M(x)$ denote the normalized margin between the two highest softmax outputs from the last trained model \mathbb{M} . Define Δ as the set of individual δ -values for each labeled example in \mathbb{L} . As in the theoretical analysis, $P[C(\mathbb{L}, \Delta)]$ denotes the probability of coverage for \mathbb{L} given Δ . The competence score $S_{\mathcal{L}}(\mathbb{L}, \Delta)$ is defined by the objective function (5). The graph $\{G_{\delta} = (V, E)\}$ is a directed adjacency graph where nodes are samples, and edges connect pairs of nodes if their distance in the embedding space is less than δ .

3.2 Active learning method

Active Learning (AL) is performed iteratively (see Fig. 1): at each iteration i , a query set Q of q unlabeled examples is selected based on a specific strategy, where q denotes the query set size and Q denotes the current query set. These examples are then labeled by an oracle, added to the labeled set \mathbb{L} , and removed from the unlabeled pool \mathbb{U} . Subsequently, the algorithm parameters may be updated as needed, depending on the specific requirements of the algorithm. This process

is repeated until the label budget is exhausted or predefined termination conditions are met.

Our AL method **DCoM** involves several distinct steps:

Step 1: Initialization. Identify an appropriate embedding space for $\mathbb{U} \cup \mathbb{L}$, where distances are expected to be inversely correlated to semantic similarity. This can be achieved using self-supervised or representation learning techniques. Select an initial radius δ_0 as outlined in (Yehuda et al. 2022), and initialize the parameter $\Delta = \emptyset$. If $\mathbb{L} \neq \emptyset$, skip *Step 2* for now and begin the iterations with *Step 3*.

Step 2: Active sampling. Select q examples from \mathbb{U} for labeling (see Alg 1 for the pseudo-code). Begin by computing the normalized margin $M(x) \forall x \in \mathbb{U}$ using the latest model \mathbb{M} . Next, construct a directed adjacency graph $\{G_{\delta_{\text{avg}}} = (V, E)\}$, where δ_{avg} is the average of Δ , or δ_0 if Δ is empty. To avoid covering points multiple times, $\forall x_i \in \mathbb{L}, \forall x \in B_{\delta_i}(x_i)$ and $\forall v \in V$, prune all incoming edges $e = (v, x) \in E$. Additionally, prune all outgoing edges $e = (x_i, v) \in E$.

Using this graph, compute the Out-Degree-Rank (ODR) $\forall x \in \mathbb{U}$. Likewise, compute the probability of coverage $P[C(\mathbb{L}, \Delta)]$ of the current \mathbb{L} and its corresponding Δ , and use these quantities to determine $S_{\mathcal{L}}(\mathbb{L}, \Delta)$. Now select q points from \mathbb{U} in a greedy manner as follows:

1. $\forall x \in \mathbb{U}$, compute the Out-Degree-Rank $\text{ODR}(x)$.

2. $\forall x \in \mathbb{U}$, compute a ranking score

$$R(x) = S_{\mathcal{L}}(\mathbb{L}, \Delta) \cdot (1 - M(x)) + (1 - S_{\mathcal{L}}(\mathbb{L}, \Delta)) \cdot \text{ODR}(x).$$

3. Select the vertex x_{\max} with the highest score

$$x_{\max} = \text{argmax}_{x \in \mathbb{U}} R(x).$$

4. Remove all incoming edges to x_{\max} and its neighbors, implying that $\text{ODR}(x_{\max}) = 0$.

5. Set $M(x_{\max}) = 1$.

Step 3: Model training: Obtain labels for the query set Q derived in *Step 2*. Remove Q from \mathbb{U} and add it to \mathbb{L} . Finally, train model \mathbb{M} using the updated \mathbb{L} (and also \mathbb{U} if the learner employs semi-supervised learning).

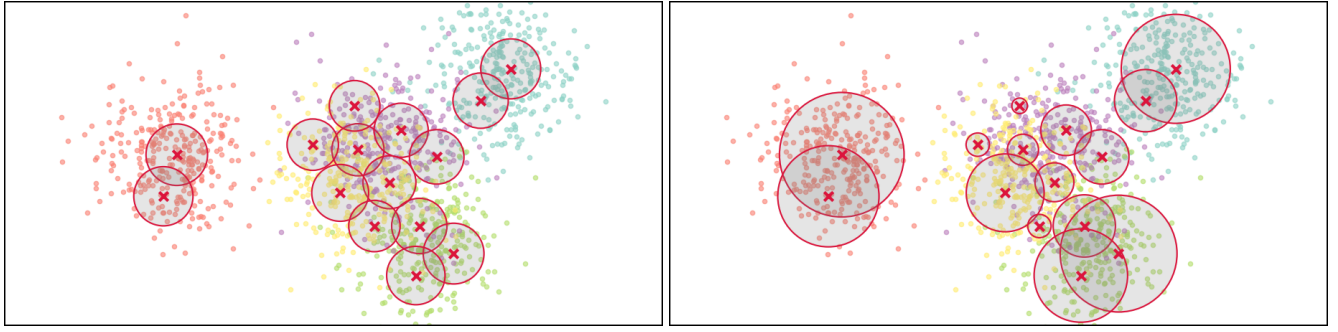
Step 4: Δ -Adjustment. Determine a suitable δ_i for each new labeled example $x_i \in Q$ and add it to Δ , see Alg 2 for pseudo-code and illustration in Fig. 2. Begin by using the updated model \mathbb{M} to predict labels for all points in the unlabeled set \mathbb{U} . Likewise, compute a purity threshold $\tau = m \cdot P[C(\mathbb{L} \setminus Q, \Delta)] + d$, where² $P[C(\mathbb{L} \setminus Q, \Delta)]$, the probability of coverage using the old labeled set, is derived in *Step 2*. Finally, for each new labeled example $v \in Q$, search for the largest radius δ_{opt} whose purity $P(\{x \in B_{\delta_{\text{opt}}}(v) : f(x) = f(v)\})$ remains above τ . Assuming that $\pi(B_{\delta}(x))$ is monotonic with δ , use binary search.

4 Empirical evaluation

4.1 Methodology

This section investigates two deep AL frameworks: a *fully supervised* approach, wherein a deep model is trained exclusively on the annotated dataset \mathbb{L} as a standard supervised

²The linear transformation defined by m, d adjusts the range of coverage scores into the relevant range of purity scores $[b, b + m]$.



(a) Initial active sampling using δ_0 in DCoM, following *ProbCover* approach.

(b) DCoM's updated Δ list, which includes a suitable δ value for each example in \mathbb{L}

Figure 2: Illustration of *Step 4: Δ -Adjustment* in DCoM, comparing the coverage obtained by DCoM (b) with ProbCover (a) using budget $b = 15$. Selected points are marked by x, and the covered area is shaded in light gray. While ProbCover maintains a constant δ for each example, DCoM seeks to maximize coverage while preserving the purity of the balls by fitting a suitable radius for each center.

Algorithm 1: DCoM, Active sampling

Input: unlabeled pool \mathbb{U} , labeled pool \mathbb{L} , query size q , list of ball sizes Δ , trained model \mathbb{M} if $\mathbb{L} \neq \emptyset$
Output: a set of points to query, and the coverage of \mathbb{L}

- 1: $\forall x \in \mathbb{U}, M(x) \leftarrow$ normalized margin between the two highest softmax outputs of \mathbb{M} if $\mathbb{L} \neq \emptyset$, 1 otherwise
- 2: Compute $P[C(\mathbb{L}, \Delta)]$
- 3: Compute $S_{\mathcal{L}}(\mathbb{L}, \Delta)$
- 4: $\delta_{\text{avg}} \leftarrow \text{Average}(\Delta)$
- 5: $G = (V = \mathbb{U} \cup \mathbb{L}, E = \{(x, x') : x' \in B_{\delta_{\text{avg}}}(x)\})$
- 6: **for** $(x_i, \delta_i) \in \mathbb{L} \times \Delta$ **do**
- 7: $\forall x \in B_{\delta_i}(x_i) : \forall e = (v, x) \in E$, remove e
- 8: $\forall e = (x_i, v) \in E$, remove e
- 9: **end for**
- 10: $Q \leftarrow \emptyset$
- 11: **for** $i = 1, \dots, q$ **do**
- 12: $\forall x \in \mathbb{U}, \text{ODR}(x) \leftarrow \text{Out-Degree Rank}$
- 13: $\forall x \in \mathbb{U}, R(x) \leftarrow S_{\mathcal{L}}(\mathbb{L}, \Delta) \cdot (1 - M(x)) + (1 - S_{\mathcal{L}}(\mathbb{L}, \Delta)) \cdot \text{ODR}(x)$
- 14: $x_{\text{max}} \leftarrow \{\text{argmax}_{x \in \mathbb{U}} R(x)\}$
- 15: $Q \leftarrow Q \cup \{x_{\text{max}}\}$
- 16: $\forall x \in B_{\delta_{\text{avg}}}(x_{\text{max}}) : \forall e = (v, x) \in E$, remove e
- 17: $M(x_{\text{max}}) \leftarrow 1$
- 18: **end for**
- 19: **return** $Q, P[C(\mathbb{L}, \Delta)]$

task, and a *semi-supervised* framework trained on both the annotated and unlabeled datasets, \mathbb{L} and \mathbb{U} . Our experimental setup is based on the codebase of (Munjal et al. 2022), ensuring a fair comparison among the various AL strategies by using the same network architectures while sharing all the relevant experimental conditions.

More specifically, we trained ResNet-18 (He et al. 2016) on the following benchmark datasets: STL-10 (Coates, Ng, and Lee 2011), SVHN (Netzer et al. 2011), CIFAR-100 (Krizhevsky, Hinton et al. 2009) and subsets of ImageNet (Deng et al. 2009) including ImageNet-50, ImageNet-100, and ImageNet-200 as defined in (Van Gansbeke et al. 2020). The hyper-parameters are detailed in Appendix A. In the semi-supervised framework, we used FlexMatch (Zhang et al.

Algorithm 2: DCoM, Δ -Adjustment

Input: unlabeled pool \mathbb{U} , labeled pool \mathbb{L} , query pool Q , maximal ball size δ_{max} , list of ball sizes Δ for $\mathbb{L} \setminus Q$, trained model \mathbb{M} from the current iteration and $P[C(\mathbb{L} \setminus Q, \Delta)]$ from Step 2
Output: updated list of ball sizes Δ

- 1: $\tau \leftarrow m \cdot P[C(\mathbb{L} \setminus Q, \Delta)] + d$
- 2: $\hat{Y} \leftarrow$ The predicted label for each $x \in \mathbb{U}$ using the model \mathbb{M}
- 3: **for** $v \in Q$ **do**
- 4: $\delta_{\text{opt}} \leftarrow \text{argmax}_{\delta} [P(\{x \in B_{\delta}(v) : f(x) = f(v)\}) > \tau]$
- 5: $\Delta \leftarrow \Delta + [\delta_{\text{opt}}]$
- 6: **end for**
- 7: **return** Δ

2021) and the code provided by (Wang et al. 2022), adopting the parameters specified by (Zhang et al. 2021) (see details in Appendix A). While the ResNet-18 architecture may no longer achieve state-of-the-art results on the datasets examined, it serves as a suitable platform to evaluate the efficacy of AL strategies in a competitive and fair environment, where they have demonstrated benefits.

In our comparisons, we used several active learning strategies for selecting a query set: (i) *Random* sampling, (ii) *Min margin* — lowest margin between the two highest softmax outputs; (iii) *Max entropy* — highest entropy of softmax outputs; (iv) *Uncertainty* — 1 minus the highest softmax output; (v) *DBAL* (Gal, Islam, and Ghahramani 2017); (vi) *CoreSet* (Sener and Savarese 2018); (vii) *BALD* (Kirsch, Van Amersfoort, and Gal 2019); (viii) *BADGE* (Ash et al. 2019); (ix) *ProbCover* (Yehuda et al. 2022); and (x) *LDM-s* (Cho et al. 2023). When available, we used the code provided in (Munjal et al. 2022) for each strategy. When it was unavailable, we used the code from the repositories of the corresponding papers. Since (Cho et al. 2023) doesn't provide code, we compared our results with the corresponding available results reported in their paper, despite differences in the running setup (see Appendix E.5).

DCoM and ProbCover require a suitable data embedding. For STL-10, SVHN, CIFAR-10 and CIFAR-100 we employed the SimCLR (Chen et al. 2020) embedding. For the ImageNet subsets we used the DINOv2 (Oquab et al. 2023)

embedding. Section 4.3 provides an extensive ablation study, which includes alternative embedding spaces. In all experiments, identical settings and hyper-parameters are used as detailed in Appendix A. The robustness of our method to these choices is discussed in Appendix C.

Using a sparse representation of the adjacency graph enables *DCoM* to handle large datasets efficiently without exhaustive space requirements. The algorithm’s complexity, including adjacency graph construction and sample selection, is discussed in Appendix D.

4.2 Main results

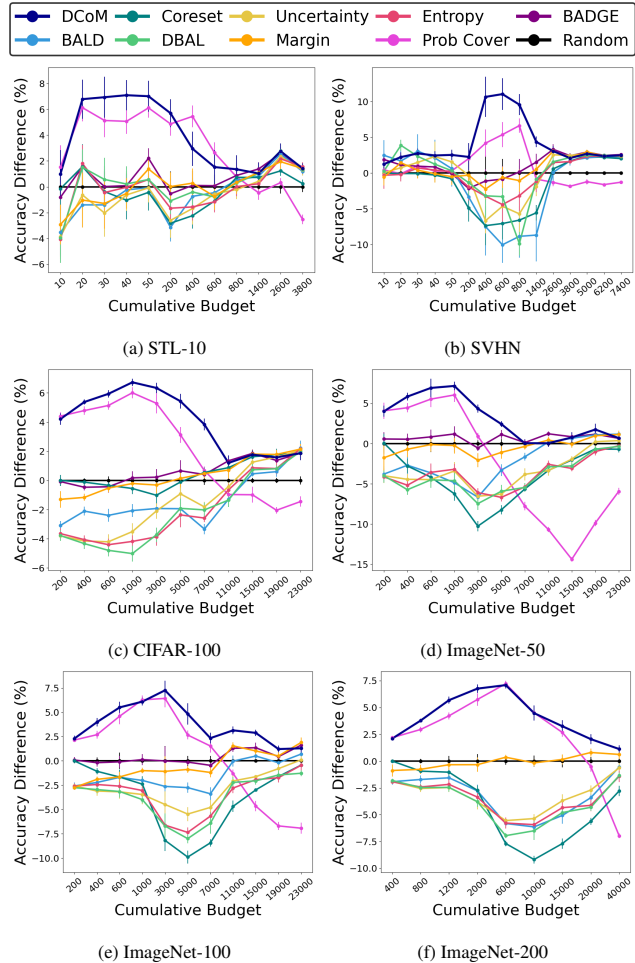


Figure 3: Mean accuracy difference between AL algorithms and random queries. Positive mean difference indicates that the corresponding AL method is beneficial. The errors bars correspond to standard error, using 5-10 repetitions (3 for the ImageNet subsets). While some methods perform well only in specific budget regime, *DCoM* consistently achieves the best results across all budgets. Cumulative budget is evenly spaced for easy range comparison.

Fully supervised framework. We evaluate various AL methods by training a ResNet-18 model from scratch for each different AL strategy, using the labels of the queries selected by the respective method. In each AL iteration, a new model

is trained from scratch using the updated labeled set \mathbb{L} . This process is repeated for several AL iterations. Fig. 3 shows the difference between the accuracy obtained by each AL method, and the accuracy obtained when training a similar network with a random query set of the same size (the baseline of no active learning), for each AL iteration. The final accuracy of each method is shown in Table 1 for the CIFAR-100 dataset, as mean \pm Standard Error (STE). Similar tables for the remaining datasets are shown in Appendix E.

Semi-supervised framework. We evaluate the effectiveness of 5 representative AL strategies with FlexMatch, a competitive semi-supervised learning method. We also evaluate our method, and the results of random sampling (no AL) as baseline. Fig. 4 shows the mean accuracy and STE based on 3 repetitions of FlexMatch, employing labeled sets generated by the different AL strategies. Note that in these experiments, since the query is selected from an unlabeled set, the resulting labeled set \mathbb{L} may be unbalanced between the classes, which is especially harmful when the budget is small. This affects all the methods. As a result, the accuracy with random sampling may differ from reported results. Notably, *DCoM* demonstrates significant superiority over random sampling.

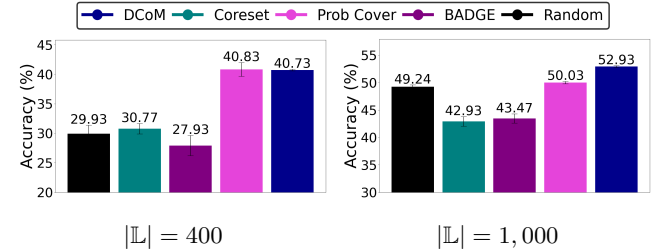


Figure 4: Comparison of AL strategies in a semi-supervised learning framework. Each bar shows the mean test accuracy over 3 repetitions of FlexMatch, trained with 400 and 1,000 labeled examples on CIFAR-100. Three AL rounds are conducted, selecting 100, 300, and 600 examples in each round.

4.3 Ablation study

We present a series of experiments where we investigate the choices made by our method, including different feature spaces and different uncertainty-based measures. The results demonstrate the robustness of our method to these choices. Additional choices are investigated in Appendix E, including the contribution of a dynamic δ and initialization δ_0 (Appendix E.1). In Appendix E.3, we evaluate the effectiveness of $S_{\mathcal{L}}(\mathbb{L}, \Delta)$ from (5) in capturing competence.

Different feature spaces. As discussed in Section 3, our approach relies on the existence of a suitable embedding space, where distance is indicative of semantic dissimilarity. We now repeat the basic fully-supervised experiments while varying the embedding space, comparing various popular self-supervised representations. Results are reported in Fig. 5, showing that *DCoM* consistently delivers the best performance regardless of the specific embedding used.

Breaking down the algorithm into its components. The objective function in (1) includes the linear combination of two

$ \mathbb{L} $	Random	Prob Cover	BADGE	BALD	Coreset	Uncertainty	Entropy	DBAL	Margin	LDM-s	DCoM
200	6.39 \pm 0.19	10.79\pm0.08	6.31 \pm 0.09	3.30 \pm 0.11	6.39 \pm 0.19	2.59 \pm 0.05	2.74 \pm 0.17	2.61 \pm 0.18	5.09 \pm 0.37	-	10.59\pm0.19
400	8.74 \pm 0.07	13.53 \pm 0.22	8.27 \pm 0.14	6.63 \pm 0.23	8.62 \pm 0.17	4.59 \pm 0.23	4.68 \pm 0.23	4.41 \pm 0.30	7.58 \pm 0.17	-	14.11\pm0.11
600	10.73 \pm 0.13	15.86 \pm 0.16	10.29 \pm 0.27	8.33 \pm 0.31	10.39 \pm 0.25	6.52 \pm 0.38	6.32 \pm 0.27	5.94 \pm 0.28	10.20 \pm 0.16	-	16.66\pm0.11
1,000	13.49 \pm 0.18	19.49 \pm 0.20	13.66 \pm 0.26	11.42 \pm 0.26	12.94 \pm 0.21	9.98 \pm 0.38	9.31 \pm 0.22	8.47 \pm 0.35	13.28 \pm 0.19	-	20.21\pm0.07
3,000	24.02 \pm 0.27	29.31 \pm 0.42	24.24 \pm 0.28	22.10 \pm 0.11	23.00 \pm 0.28	21.93 \pm 0.26	20.15 \pm 0.33	20.29 \pm 0.23	23.71 \pm 0.31	-	30.36\pm0.08
5,000	31.52 \pm 0.39	34.64 \pm 0.15	32.18 \pm 0.33	29.58 \pm 0.38	31.41 \pm 0.26	30.60 \pm 0.40	29.15 \pm 0.46	29.60 \pm 0.28	31.66 \pm 0.23	-	36.95\pm0.10
7,000	37.69 \pm 0.16	38.36 \pm 0.13	38.09 \pm 0.10	34.36 \pm 0.20	38.24 \pm 0.16	35.87 \pm 0.19	35.11 \pm 0.11	35.67 \pm 0.35	38.16 \pm 0.17	31.85 \pm 0.00	41.52\pm0.25
11,000	45.66 \pm 0.22	44.69 \pm 0.20	47.00\pm0.16	44.37 \pm 0.28	46.53 \pm 0.18	45.23 \pm 0.20	45.01 \pm 0.17	44.31 \pm 0.24	46.37 \pm 0.36	40.88 \pm 0.01	46.86\pm0.28
15,000	50.57 \pm 0.09	49.58 \pm 0.46	52.42\pm0.17	51.02 \pm 0.09	52.19\pm0.29	51.82 \pm 0.16	51.43 \pm 0.21	51.30 \pm 0.35	52.37\pm0.19	46.59 \pm 0.01	52.33\pm0.22
19,000	54.95 \pm 0.09	52.90 \pm 0.14	56.32 \pm 0.07	55.55 \pm 0.27	56.72\pm0.31	56.55\pm0.21	55.76 \pm 0.31	55.75 \pm 0.14	56.73\pm0.24	49.41 \pm 0.01	56.53\pm0.07
23,000	57.74 \pm 0.14	56.29 \pm 0.21	59.60\pm0.16	59.96\pm0.35	59.59\pm0.22	59.79\pm0.23	59.91\pm0.08	59.72\pm0.21	59.88\pm0.21	52.48 \pm 0.00	59.60\pm0.33

Table 1: Model accuracy with varying labeled set sizes \mathbb{L} (row) and AL strategies (column) while training directly on CIFAR-100 images.

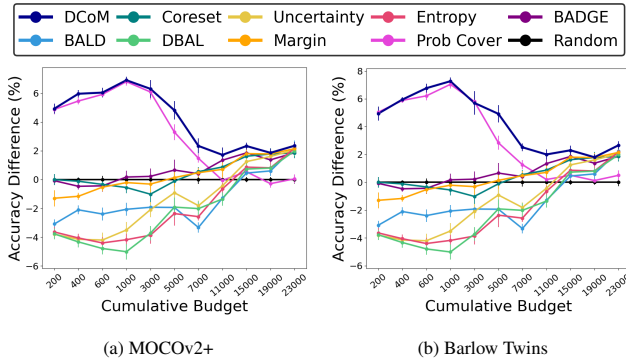


Figure 5: Performance over CIFAR-100, using two different embedding spaces for *DCoM* and *ProbCover*, see details in the caption of Fig. 3. Clearly, *DCoM* consistently achieves the best results. Results using an additional embedding space are shown in Appendix E.4.

objective functions, weighed by competence score $S_{\mathcal{L}}(\mathbb{L}, \Delta)$ from (5). We evaluate the contribution of each component in this objective function separately. Results are shown in Fig. 6, wherein *DPC* denotes the Dynamic Probability Coverage, corresponding to $\mathcal{O}_{low}(x)$ in *DCoM*, and *Margin* denotes *DCoM*'s choice for $\mathcal{O}_{high}(x)$. Clearly, the weighted objective function of *DCoM* yields superior results.

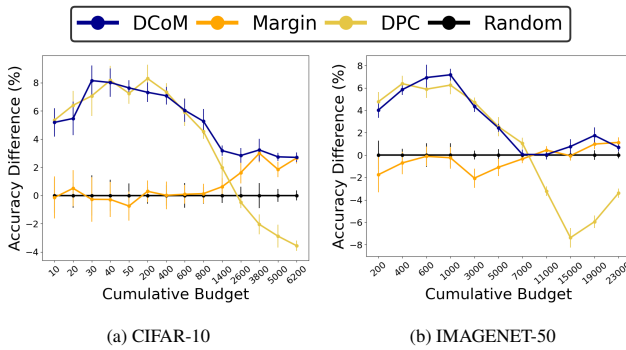


Figure 6: Performance (mean accuracy and STE) when optimizing each component of objective function (1) separately and together.

Different uncertainty-based methods. We evaluate our

choice for $\mathcal{O}_{high}(x)$ in objective function (1), investigating the alternative methods of min margin, entropy of the min max activation, and uncertainty (see details in Section 4.1). Additionally, we use a score reminiscent of the AL method *BADGE* (Gal, Islam, and Ghahramani 2017) and termed *Gradient norm*, which computes the norm of the gradient between the learner's last two layers. Once again, the results of *DCoM* show robustness to this choice, with insignificant differences between the different uncertainty scores, see Fig. 7. Consequently, we prioritize computational efficiency and opt for the fastest-to-compute score, which is min-margin.

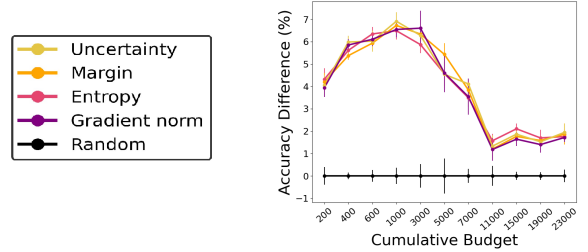


Figure 7: Similar to Fig. 3, using only *DCoM* while leveraging 4 different variants for its underlying uncertainty score (see text). The performance differences between the variants are hardly significant.

5 Summary

We investigate the challenge of Active Learning (AL) in a multi-budget setting. Our approach is motivated by a new bound on the generalization error of the Nearest Neighbor classifier, and aims to minimize this bound. Additionally, the sampling strategy is dynamically adjusted during training using a new competence score, also motivated by the same bound. We validate our method empirically in both supervised and semi-supervised frameworks across various datasets. The results show that *DCoM* significantly outperforms alternative methods across all budgetary constraints.

Acknowledgments

This work was supported by grants from the Israeli Council of Higher Education, AFOSR award FA8655-24-1-7006, and the Gatsby Charitable Foundation.

References

Ash, J. T.; Zhang, C.; Krishnamurthy, A.; Langford, J.; and Agarwal, A. 2019. Deep Batch Active Learning by Diverse, Uncertain Gradient Lower Bounds. In *International Conference on Learning Representations*.

Chen, L.; Bai, Y.; Huang, S.; Lu, Y.; Wen, B.; Yuille, A.; and Zhou, Z. 2024. Making your first choice: to address cold start problem in medical active learning. In *Medical Imaging with Deep Learning*, 496–525. PMLR.

Chen, T.; Kornblith, S.; Norouzi, M.; and Hinton, G. 2020. A simple framework for contrastive learning of visual representations. In *International conference on machine learning*, 1597–1607. PMLR.

Cho, S. J.; Kim, G.; Lee, J.; Shin, J.; and Yoo, C. D. 2023. Querying Easily Flip-flopped Samples for Deep Active Learning. In *The Twelfth International Conference on Learning Representations*.

Chowdhury, S.; Hamerly, G.; and McGarry, M. 2024. Active Learning Strategy Using Contrastive Learning and K-Means for Aquatic Invasive Species Recognition. In *Proceedings of the IEEE/CVF Winter Conference on Applications of Computer Vision (WACV) Workshops*, 848–858.

Coates, A.; Ng, A.; and Lee, H. 2011. An analysis of single-layer networks in unsupervised feature learning. In *Proceedings of the fourteenth international conference on artificial intelligence and statistics*, 215–223. JMLR Workshop and Conference Proceedings.

Cohn, D. A.; Ghahramani, Z.; and Jordan, M. I. 1996. Active learning with statistical models. *Journal of artificial intelligence research*, 4: 129–145.

da Costa, V. G. T.; Fini, E.; Nabi, M.; Sebe, N.; and Ricci, E. 2022. solo-learn: A Library of Self-supervised Methods for Visual Representation Learning. *Journal of Machine Learning Research*, 23(56): 1–6.

Deng, J.; Dong, W.; Socher, R.; Li, L.-J.; Li, K.; and Fei-Fei, L. 2009. Imagenet: A large-scale hierarchical image database. In *2009 IEEE conference on computer vision and pattern recognition*, 248–255. Ieee.

El-Hasnony, I. M.; Elzeki, O. M.; Alshehri, A.; and Salem, H. 2022. Multi-Label Active Learning-Based Machine Learning Model for Heart Disease Prediction. *Sensors*, 22(3).

Gal, Y.; Islam, R.; and Ghahramani, Z. 2017. Deep bayesian active learning with image data. In *International Conference on Machine Learning*, 1183–1192. PMLR.

Gissin, D.; and Shalev-Shwartz, S. 2019. Discriminative active learning. *arXiv preprint arXiv:1907.06347*.

Grill, J.-B.; Strub, F.; Altché, F.; Tallec, C.; Richemond, P.; Buchatskaya, E.; Doersch, C.; Avila Pires, B.; Guo, Z.; Gheshlaghi Azar, M.; et al. 2020. Bootstrap your own latent-a new approach to self-supervised learning. *Advances in neural information processing systems*, 33: 21271–21284.

Hacohen, G.; Dekel, A.; and Weinshall, D. 2022. Active Learning on a Budget: Opposite Strategies Suit High and Low Budgets. In *International Conference on Machine Learning*. PMLR.

Hacohen, G.; and Weinshall, D. 2024. How to Select Which Active Learning Strategy is Best Suited for Your Specific Problem and Budget. *Advances in Neural Information Processing Systems*, 36.

He, K.; Fan, H.; Wu, Y.; Xie, S.; and Girshick, R. 2020. Momentum contrast for unsupervised visual representation learning. In *Proceedings of the IEEE/CVF conference on computer vision and pattern recognition*, 9729–9738.

He, K.; Zhang, X.; Ren, S.; and Sun, J. 2016. Deep Residual Learning for Image Recognition. In *2016 IEEE Conference on Computer Vision and Pattern Recognition, CVPR 2016, Las Vegas, NV, USA, June 27-30, 2016*, 770–778. IEEE Computer Society.

Houlsby, N.; Huszár, F.; Ghahramani, Z.; and Lengyel, M. 2011. Bayesian Active Learning for Classification and Preference Learning. *stat*, 1050: 24.

Hu, R.; Mac Namee, B.; and Delany, S. J. 2010. Off to a good start: Using clustering to select the initial training set in active learning. In *Twenty-Third International FLAIRS Conference*.

Jung, S.; Kim, S.; and Lee, J. 2023. A simple yet powerful deep active learning with snapshot ensembles. In *The Eleventh International Conference on Learning Representations*. International Conference on Learning Representations.

Kaseb, A.; and Farouk, M. 2023. Active learning for Arabic sentiment analysis. *Alexandria Engineering Journal*, 77: 177–187.

Kim, K.; Park, D.; Kim, K. I.; and Chun, S. Y. 2021. Task-Aware Variational Adversarial Active Learning. In *2021 IEEE/CVF Conference on Computer Vision and Pattern Recognition (CVPR)*, 8162–8171. IEEE.

Kirsch, A.; Van Amersfoort, J.; and Gal, Y. 2019. Batchbald: Efficient and diverse batch acquisition for deep bayesian active learning. *Advances in neural information processing systems*, 32: 7026–7037.

Krizhevsky, A.; Hinton, G.; et al. 2009. Learning multiple layers of features from tiny images. *Online*.

Lewis, D. D.; and Gale, W. A. 1994. A sequential algorithm for training text classifiers. In *Proceedings of the 17th annual international ACM SIGIR conference on Research and development in information retrieval*, 3–12.

Munjal, P.; Hayat, N.; Hayat, M.; Sourati, J.; and Khan, S. 2022. Towards Robust and Reproducible Active Learning using Neural Networks. In *2022 IEEE/CVF Conference on Computer Vision and Pattern Recognition (CVPR)*, 223–232. IEEE.

Netzer, Y.; Wang, T.; Coates, A.; Bissacco, A.; Wu, B.; Ng, A. Y.; et al. 2011. Reading digits in natural images with unsupervised feature learning. In *NIPS workshop on deep learning and unsupervised feature learning*, 5, 7. Granada, Spain.

Oquab, M.; Darcret, T.; Moutakanni, T.; Vo, H. V.; Szafraniec, M.; Khalidov, V.; Fernandez, P.; HAZIZA, D.; Massa, F.; El-Nouby, A.; et al. 2023. DINOv2: Learning Robust Visual Features without Supervision. *Transactions on Machine Learning Research*.

Parvaneh, A.; Abbasnejad, E.; Teney, D.; Haffari, G. R.; Van Den Hengel, A.; and Shi, J. Q. 2022. Active learning by feature mixing. In *Proceedings of the IEEE/CVF conference on computer vision and pattern recognition*, 12237–12246.

Ranganathan, H.; Venkateswara, H.; Chakraborty, S.; and Panchanathan, S. 2017. Deep active learning for image classification. In *2017 IEEE International Conference on Image Processing (ICIP)*, 3934–3938.

Schmidt, S.; Schenk, L.; Schwinn, L.; and Günnemann, S. 2024. A Unified Approach Towards Active Learning and Out-of-Distribution Detection. *arXiv:2405.11337*.

Sener, O.; and Savarese, S. 2018. Active Learning for Convolutional Neural Networks: A Core-Set Approach. In *International Conference on Learning Representations*.

Settles, B. 2009. Active learning literature survey. Technical report, University of Wisconsin-Madison Department of Computer Sciences.

Shannon, C. E. 1948. A Mathematical Theory of Communication. *The Bell System Technical Journal*, 27: 379–423.

Siddhant, A.; and Lipton, Z. C. 2018. Deep Bayesian Active Learning for Natural Language Processing: Results of a Large-Scale Empirical Study. In *Proceedings of the 2018 Conference on Empirical Methods in Natural Language Processing*, 2904–2909.

Tharwat, A.; and Schenck, W. 2023. A survey on active learning: state-of-the-art, practical challenges and research directions. *Mathematics*, 11(4): 820.

Van Gansbeke, W.; Vandenhende, S.; Georgoulis, S.; Proesmans, M.; and Van Gool, L. 2020. Scan: Learning to classify images without labels. In *European conference on computer vision*, 268–285. Springer.

Wang, H.; Jin, Q.; Li, S.; Liu, S.; Wang, M.; and Song, Z. 2023. A comprehensive survey on deep active learning and its applications in medical image analysis. *arXiv preprint arXiv:2310.14230*.

Wang, Y.; Chen, H.; Fan, Y.; Sun, W.; Tao, R.; Hou, W.; Wang, R.; Yang, L.; Zhou, Z.; Guo, L.-Z.; Qi, H.; Wu, Z.; Li, Y.-F.; Nakamura, S.; Ye, W.; Savvides, M.; Raj, B.; Shinohzaki, T.; Schiele, B.; Wang, J.; Xie, X.; and Zhang, Y. 2022. USB: A Unified Semi-supervised Learning Benchmark for Classification. In *Thirty-sixth Conference on Neural Information Processing Systems Datasets and Benchmarks Track*.

Wen, Z.; Pizarro, O.; and Williams, S. 2023. NTKCPL: Active Learning on Top of Self-Supervised Model by Estimating True Coverage. *arXiv e-prints*, arXiv-2306.

Woo, J. O. 2022. Active Learning in Bayesian Neural Networks with Balanced Entropy Learning Principle. In *The Eleventh International Conference on Learning Representations*.

Xie, Y.; Lu, H.; Yan, J.; Yang, X.; Tomizuka, M.; and Zhan, W. 2023. Active finetuning: Exploiting annotation budget in the pretraining-finetuning paradigm. In *Proceedings of the IEEE/CVF Conference on Computer Vision and Pattern Recognition*, 23715–23724.

Yang, Y.; Ma, Z.; Nie, F.; Chang, X.; and Hauptmann, A. 2015. Multi-Class Active Learning by Uncertainty Sampling with Diversity Maximization. *International Journal of Computer Vision*, 113.

Yehuda, O.; Dekel, A.; Hacohen, G.; and Weinshall, D. 2022. Active learning through a covering lens. *Advances in Neural Information Processing Systems*, 35: 22354–22367.

Yuan, D.; Chang, X.; Liu, Q.; Yang, Y.; Wang, D.; Shu, M.; He, Z.; and Shi, G. 2023. Active learning for deep visual tracking. *IEEE Transactions on Neural Networks and Learning Systems*.

Zbontar, J.; Jing, L.; Misra, I.; LeCun, Y.; and Deny, S. 2021. Barlow twins: Self-supervised learning via redundancy reduction. In *International conference on machine learning*, 12310–12320. PMLR.

Zhang, B.; Wang, Y.; Hou, W.; Wu, H.; Wang, J.; Okumura, M.; and Shinohzaki, T. 2021. Flexmatch: Boosting semi-supervised learning with curriculum pseudo labeling. *Advances in Neural Information Processing Systems*, 34: 18408–18419.

Zhao, G.; Dougherty, E.; Yoon, B.-J.; Alexander, F.; and Qian, X. 2021. Uncertainty-aware Active Learning for Optimal Bayesian Classifier. In *International Conference on Learning Representations*.

Appendix

A Implementation details

The source code for this study can be found in the zip file included in the supplementary material. This zip file contains a USAGE.md file that provides instructions on how to run the algorithm. The code in the zip file is based on the GitHub repositories of Yehuda et al. (2022) and Munjal et al. (2022). Our GitHub repository will be made public upon acceptance.

DCoM necessitates the computation of the initial delta for each dataset representation. The values utilized in our experiments can be found in Table 2. The δ values of CIFAR-10 and CIFAR-100 are sourced from (Yehuda et al. 2022). Information on the computation of δ values for other datasets can be located in Appendix E.1.

Dataset	SSL method	δ_0
STL-10	SimCLR	0.55
SVHN	SimCLR	0.4
CIFAR-10	SimCLR	0.75
CIFAR-100	SimCLR	0.65
ImageNet-50	DINOv2	0.75
ImageNet-100	DINOv2	0.7
ImageNet-200	DINOv2	0.65
CIFAR-100	MOCov2+	0.5
CIFAR-100	BYOL	0.5
CIFAR-100	Barlow Twins	0.55

Table 2: Initial delta values used in experiments

Additionally, throughout our experiments we used identical algorithm parameters, distinguishing between those for datasets with smaller class amounts (10) and larger

ones (50+). These parameters encompass the adaptive purity threshold τ from Alg 2 and the logistic function parameters for the competence score $S_{\mathcal{L}}(\mathbb{L}, \Delta)$ in (5), (a, k) . Specifically, we employed $\tau = 0.2$ cover + 0.4, with logistic parameters $a = 0.9$ and $k = 30$ for CIFAR-10, SVHN, and STL-10, and $a = 0.8$ and $k = 30$ for CIFAR-100 and ImageNet subsets. The δ resolution for the binary search in $DCoM$ was set to 0.05. Our ablation study, detailed in Appendix C, demonstrates that these selections have negligible impact on performance.

A.1 Supervised training

When training on STL-10, SVHN, CIFAR-10 and CIFAR-100 datasets, we utilized a ResNet-18 architecture trained for 200 epochs. Our optimization strategy involved using an SGD optimizer with a Nesterov momentum of 0.9, weight decay set to 0.0003, and cosine learning rate scheduling starting at a base rate of 0.025. Training was performed with a batch size of 100 examples, and we applied random cropping and horizontal flips for data augmentation. For an illustration of these parameters in use, refer to (Munjal et al. 2022).

When training ImageNet-50, we used the same hyper-parameters, only changing the base learning rate to 0.01, the batch size to 50 and the epoch amount to 50.

When training ImageNet-100/200, we used the same hyper-parameters as ImageNet-50, only changing the epoch amount to 100.

The train and test partitions followed the original sets from the corresponding paper, with 10% of the train set used for validation in all datasets except for ImageNet-200, where 5% was used for validation.

A.2 Semi-supervised training

When training FlexMatch (Zhang et al. 2021), we used the semi supervised framework by (Wang et al. 2022), and the AL framework by (Munjal et al. 2022). All experiments involved 3 repetitions.

We relied on the standard hyper-parameters used by FlexMatch (Zhang et al. 2021). Specifically, we trained WideResNet-28 for 512 epochs using the SGD optimizer, with 0.03 learning rate, 64 batch size, 0.9 SGD momentum, 0.999 EMA momentum, 0.001 weight decay and 2 widen factor.

A.3 Self-supervised feature extraction

STL-10, SVHN, CIFAR-10, CIFAR-100. To extract semantically meaningful features, we trained SimCLR using the code provided by (Van Gansbeke et al. 2020) for STL-10, SVHN, CIFAR-10 and CIFAR-100. Specifically, we used ResNet-18 (He et al. 2016) with an MLP projection layer to a 128-dim vector, trained for 512 epochs. All the training hyper-parameters were identical to those used by SCAN (all details can be found in (Van Gansbeke et al. 2020)). After training, we used the 512 dimensional penultimate layer as the representation space.

Representation learning: ImageNet-50/100/200. We extracted features from the official (ViT-S/14) DINOv2 weights pre-trained on ImageNet (Oquab et al. 2023). We employed

the L2-normalized penultimate layer for the embedding, which has a dimensionality of 384.

Ablation embeddings – CIFAR-100. We extracted more features as BYOL (Grill et al. 2020), MOCOV2+ (He et al. 2020), and Barlow Twins (Zbontar et al. 2021) using pre-trained weights from (da Costa et al. 2022).

B Purity Calculation in nNN

When transitioning from 1NN to nNN, the structure of the problem remains unchanged, with the key difference being that the radius δ is adjusted for each labeled example. Next, we demonstrate that the purity of each ball in the nNN problem can be precisely computed using these δ -values. This is because when a labeled example $c \in \mathbb{L}$ assigns a label to a point x , it must also cover x . Therefore, any mislabeling by c would reduce the purity, as illustrated by the following statement:

Proposition. If $c \in \mathbb{L}$ is labeling x and $x \in C(\mathbb{L}, \Delta)$, then $x \in B_{\delta_c}(c)$.

Proof. Let $c \in \mathbb{L}$ be the nearest neighbor (nNN) of x , and let δ_c be the corresponding radius for c . By definition, $f^{nNN}(x) = f(x)$, and since c is labeled, we have $f(c) = f^{nNN}(c) \equiv f^N(c)$.

Given that $x \in C(\mathbb{L}, \Delta)$, there exists a labeled example $c' \in \mathbb{L}$ that covers x , meaning $d(x, c') < \delta_{c'}$. Suppose that $c \neq c'$. Since c is the nNN of x , it follows that:

$$\frac{d(x, c)}{\delta_c} < \frac{d(x, c')}{\delta_{c'}}$$

Given $d(x, c') < \delta_{c'}$, we get:

$$\frac{d(x, c)}{\delta_c} < 1 \Rightarrow d(x, c) < \delta_c$$

Thus, $x \in B_{\delta_c}(c)$, meaning c covers x within the radius δ_c .

This implies that if x were wrongly labeled, c would still cover x , indicating lower purity in $B_{\delta_c}(c)$. \square

C Hyper-parameters exploring

Theoretical basis for the Choice of a and k . The parameter a represents the center of the sigmoid function. Our objective is for the algorithm to assign increased weight to \mathcal{O}_{high} only after it has covered a substantial portion of the dataset. Consequently, we choose $a \in (0.5, 1)$. The parameter k controls the steepness of the sigmoid curve. The function must yield 0 in the absence of coverage and approach 1 as coverage becomes complete. To achieve this, we configure the numerator of the fraction to be equal to the denominator when the cover's probability is 1. Although the function cannot pass precisely through $(0, 0)$, it can asymptotically approach $(0, \varepsilon)$ for an infinitesimally small $\varepsilon \in \mathbb{R}$.

We now investigate the relationship between this approximation error and the parameter k . Define the function $f(x)$ as $S_{\mathcal{L}}$ for simplicity:

$$f(x) = \frac{1 + e^{-k(1-a)}}{1 + e^{-k(x-a)}}$$

The limit of $f(x)$ as x approaches 0 is

$$\lim_{x \rightarrow 0} f(x) = \frac{1 + e^{-k(1-a)}}{1 + e^{ka}}$$

For the function to approach 0, we require:

$$\frac{1 + e^{-k(1-a)}}{1 + e^{ka}} \ll 1$$

This implies:

$$\begin{aligned} 1 + e^{-k(1-a)} &\ll 1 + e^{ka} \\ e^{-k(1-a)} &\ll e^{ka} \\ e^{-k} &\ll e^{ka} \\ e^{-k} &\ll 1 \end{aligned} \quad (*)$$

Next, we calculate $f(0)$:

$$f(0) = \frac{1 + e^{-k(1-a)}}{1 + e^{ka}} = \varepsilon$$

Solving for k :

$$\begin{aligned} 1 + e^{-k(1-a)} &= \varepsilon(1 + e^{ka}) \\ 1 - \varepsilon &= \varepsilon e^{ka} - e^{-k(1-a)} \\ 1 - \varepsilon &= e^{ka}(\varepsilon - e^{-k}) \\ e^{ka} &= \frac{1 - \varepsilon}{\varepsilon - e^{-k}} \end{aligned}$$

Approximating e^{ka} using $(*)$:

$$e^{ka} \approx \frac{1 - \varepsilon}{\varepsilon}$$

So:

$$ka \approx \ln\left(\frac{1 - \varepsilon}{\varepsilon}\right)$$

Finally:

$$k \approx \frac{1}{a} \ln\left(\frac{1}{\varepsilon} - 1\right) \approx \frac{\ln\left(\frac{1}{\varepsilon}\right)}{a}$$

To minimize the approximation error, we should choose a larger k . In our experiments with $a = 0.8$ or 0.9 and $\varepsilon = 10^{-10}$, we determined:

$$k(a = 0.9, \varepsilon = 10^{-10}) \approx 25.58$$

$$k(a = 0.8, \varepsilon = 10^{-10}) \approx 28.78$$

The value of ε was chosen to be asymptotically smaller than the dimension of the initial graphs constructed for all the datasets. In accordance, we chose $k = 30$.

Experimental assessment of $DCoM$ hyper-parameter consistency As described before, $DCoM$ has 3 hyper-parameters: a, k and τ . When running the main experiments described in Section 4.2, we maintained consistency by employing identical parameters for STL-10, SVHN, and CIFAR-10, as well as for CIFAR-100 and the subsets of ImageNet. This approach helps to demonstrate that the choice of the hyper-parameters is not critical and does not significantly affect the results. Here, we conduct experiments with $DCoM$ using STL-10 and CIFAR-100 datasets and several values for a and k from the definition of the competence score $S_{\mathcal{L}}(\mathbb{L}, \Delta)$ in (5). We observe that while certain choices may be slightly better than others, all choices yield similar results, and $DCoM$ consistently outperforms or matches the performance of previous methods.

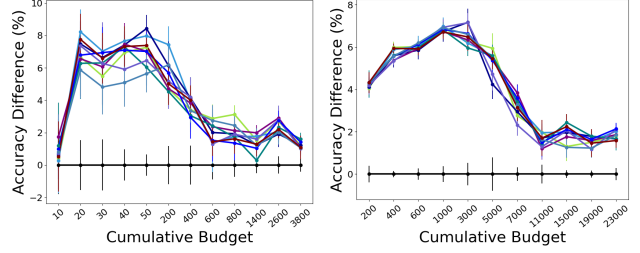
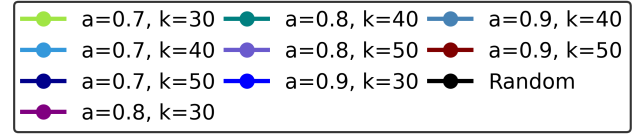


Figure 8: Evaluation of $DCoM$ across different settings of the logistic function hyper-parameters a and k . Each plot displays the mean and standard error over 3 – 5 repetitions. The findings indicate that fine-tuning these parameters has negligible effects on performance.

D Time and space complexity of $DCoM$

For the complexity analysis below, let n represent the number of examples in the combined unlabeled and labeled pool $|\mathbb{U} \cup \mathbb{L}|$, d the dimension of the data embedding space, b – the given budget ($|\mathbb{L}|$) and q – the size of the query set. As previously stated, $DCoM$ can be divided into three distinct steps:

D.1 Selection of initial δ delta

Time Complexity: The process begins by creating t adjacency graphs, each corresponding to a different δ value being evaluated. Here, t denotes the number of δ 's being examined. The time complexity of each graph generation is $O(n^2 \cdot d)$ time. The computation of purity requires the prediction of pseudo-labels by k-means at a cost of $O(n^2)$. The complexity of computing ball purity for one example is $O(n^2)$, so totally the ball purity computing for one graph takes $O(n^3)$. This adds up to overall time complexity of $O(tdn^2 + n^2 + tn^3) = O(tn^3)$. We can construct the initial graph using the largest δ -value and then, instead of building a new graph for each δ -value in $O(tdn^2)$, we can filter distances above the current δ in $O(dn^2 + n^2)$. However, the total complexity remains $O(tn^3)$. Although it may seem significant, this step doesn't occur during the active learning algorithm process. Additionally, it's possible to confine the data employed for purity computation to the densest points, effectively lowering the complexity to $O(dn^2)$. This approach mandates the use of at least the number of points equivalent to the number of classes for purity computation. This technique yields similar δ_0 values (consistent for CIFAR-10, CIFAR-100, and ImageNet-50, and with a variation of 0.05 for ImageNet-100/200 and STL-10 and 0.15 for SVHN).

Space complexity: Naively, the space complexity is $O(n^2)$, which might be impractical for large datasets like ImageNet. However, (Yehuda et al. 2022) demonstrates that utilizing a sparse matrix in coordinate list (COO) format and using limited δ values, the space complexity becomes $O(|E|)$, where

E represents the set of edges in the graph. Although $O(|E|)$ remains $O(n^2)$ in the worst-case scenario, in practice, the average vertex degree with a limited radius is less than n .

D.2 Δ -Adjustment

Time complexity: Each iteration of *DCoM* starts with customizing δ values for each labeled example from the last active step. In the worst case, there are $|\mathbb{L}|$ examples. Customizing Δ involves building the adjacency graph using δ_{\max} , running all examples on the model to obtain their predictions, and applying binary search over δ values between 0 and δ_{\max} for each example from the last active step. The binary search is performed on a continuous parameter (δ) with a search resolution r . This implies that there are $\frac{\delta_{\max}}{r}$ available values for δ . For each δ value, the algorithm computes its purity value. Overall, this process takes $O(dn^2 + n + |\mathbb{L}| \cdot \log(\frac{\delta_{\max}}{r}) \cdot n^2) = O(dn^2 + b \cdot \log(\frac{\delta_{\max}}{r}) \cdot n^2)$. In practical terms, due to the vectorization of these processes, it requires approximately 27 minutes to construct an adjacency graph for ImageNet-200 and update deltas for 1000 examples on a single CPU.

Space complexity: Similar to the space complexity analysis in Appendix D.1, which is $O(n^2)$.

D.3 Active sampling

Time complexity: Active sampling involves balancing model min-margin and example density based on the current adjacency graph. Initially, the margin of each example is computed using the softmax output from the model’s last layer, requiring $O(n)$ time. Subsequently, the current adjacency is created using δ_{avg} , which is the average over the \mathbb{L} δ values list - Δ . As discussed in Appendix D.1, this step has a time complexity of $O(dn^2)$. Following this, the iterative process for selecting a single sample includes the following steps:

- Calculating node degrees - $O(|E|)$ time.
- Finding the node with maximal degree - $O(n)$ time.
- Removing incoming edges from the graph for covered points - $O(|E|)$ time.

Samples are iteratively selected from the current sparse graph, with incoming edges to newly covered samples being removed. Unlike adjacency graph creation, sample selection cannot be parallelized, as each step depends on the previous one. Overall, the time complexity for selecting a sample is $O(|E| + n)$, resulting in a worst-case overall complexity of $O(dn^2)$. However, as more points are selected, the removal of edges speeds up the selection of later samples. Practically, it consumes about 15 minutes to construct an adjacency graph and select 1000 samples from ImageNet-200 on a single CPU.

Space complexity: Similar to the previous space complexity analysis - $O(n^2)$.

E Additional empirical results

E.1 δ_0 Initialization

To set the initial value δ_0 , we adopted the method outlined in (Yehuda et al. 2022), as detailed in Section 3. Fig. 9 displays

the purity function across various δ values, along with the selected δ values for each dataset. As mentioned previously, the δ values for CIFAR-10 and CIFAR-100 are derived from (Yehuda et al. 2022).

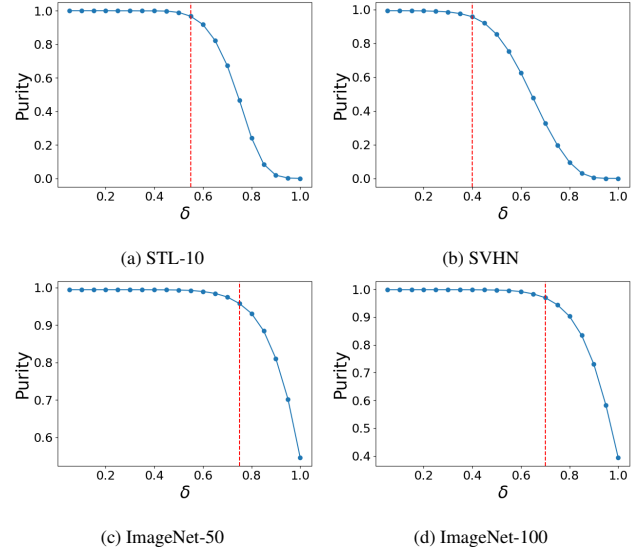


Figure 9: $\pi(\delta)$, estimated from the unlabeled data and using k-means algorithm for labeling. The dashed line indicates the highest δ , after which purity drops below $\alpha = 0.95$.

E.2 Δ distribution evolution throughout training

The experiment in Fig. 10 illustrates the distribution of Δ throughout the active selection and training phases of *DCoM*. The significant standard deviation of Δ compared to the minor standard error underscores the significance of employing a dynamic method that assigns a distinct radius to each ball.

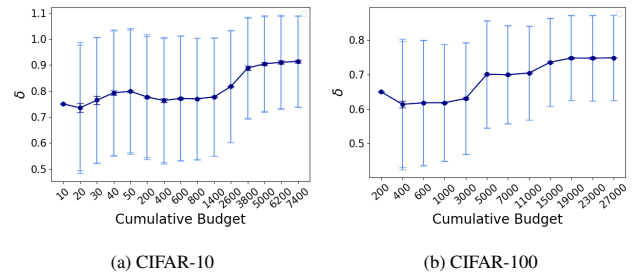


Figure 10: The Δ distribution through *DCoM* algorithm. Each plot displays the distribution over 5-10 repetitions. The results indicate that as the emphasis shifts towards maximizing the purity of sample balls, rather than solely focusing on maximum coverage, the radii adapt accordingly. This, combined with the improved performance observed with *DCoM*, highlights the necessity of the dynamic algorithm in enhancing the effectiveness of active sampling.

E.3 Empirical evaluation of $S_{\mathcal{L}}$

Fig. 11 tracks the behavior of the competence score $S_{\mathcal{L}}$ across 3 datasets. In all cases, the comparison of Figs.11a,11b reveals that $S_{\mathcal{L}}$ increases monotonically with competence as

$ \mathbb{L} $	Random	Prob Cover	BADGE	BALD	Coreset	Uncertainty	Entropy	DBAL	Margin	LDM-s	DCoM
10	14.53 \pm 0.60	20.39\pm0.23	15.17 \pm 0.94	10.81 \pm 0.61	14.65 \pm 0.74	12.99 \pm 0.77	12.78 \pm 0.72	11.74 \pm 0.69	14.39 \pm 0.88	-	19.72 \pm 0.40
20	16.82 \pm 0.44	24.64\pm0.73	17.85 \pm 0.77	13.79 \pm 0.89	16.09 \pm 0.74	16.38 \pm 0.52	17.07 \pm 0.62	17.00 \pm 0.49	17.33 \pm 0.85	-	22.28 \pm 0.75
30	18.82 \pm 0.71	27.19\pm0.25	20.38 \pm 0.67	16.25 \pm 0.83	18.22 \pm 0.93	18.00 \pm 0.68	19.26 \pm 0.44	18.34 \pm 0.50	18.55 \pm 0.87	-	26.98\pm0.35
40	20.89 \pm 0.55	29.46\pm0.38	22.19 \pm 0.45	17.93 \pm 0.67	19.79 \pm 0.61	19.00 \pm 0.70	19.98 \pm 0.60	20.30 \pm 0.35	20.61 \pm 0.68	-	28.91\pm0.46
50	22.75 \pm 0.42	29.80 \pm 0.21	22.41 \pm 0.35	18.36 \pm 0.54	21.26 \pm 0.63	21.63 \pm 0.70	22.17 \pm 0.48	21.06 \pm 0.45	22.00 \pm 0.61	-	30.39\pm0.12
200	31.53 \pm 0.29	38.83\pm0.18	32.10 \pm 0.42	27.95 \pm 0.29	30.91 \pm 0.76	30.69 \pm 0.27	29.51 \pm 0.42	28.91 \pm 0.50	31.83 \pm 0.48	-	38.86\pm0.40
400	38.64 \pm 0.36	45.36\pm0.51	37.92 \pm 0.37	35.10 \pm 0.33	37.85 \pm 0.70	36.48 \pm 0.46	36.71 \pm 0.38	36.01 \pm 0.32	38.65 \pm 0.62	-	45.72\pm0.27
600	43.66 \pm 0.44	49.13\pm0.36	42.69 \pm 0.35	40.75 \pm 0.29	42.48 \pm 0.39	41.96 \pm 0.24	40.75 \pm 0.23	41.19 \pm 0.53	43.75 \pm 0.22	-	49.71\pm0.39
800	46.84 \pm 0.29	51.49\pm0.37	46.34 \pm 0.32	44.12 \pm 0.49	46.21 \pm 0.25	45.50 \pm 0.17	43.89 \pm 0.31	44.93 \pm 0.42	46.97 \pm 0.40	-	52.10\pm0.58
1,400	54.35 \pm 0.27	56.33 \pm 0.26	54.06 \pm 0.42	53.08 \pm 0.34	52.31 \pm 0.31	53.13 \pm 0.28	52.93 \pm 0.34	53.28 \pm 0.50	54.97 \pm 0.35	50.30 \pm 0.00	57.54\pm0.10
2,600	62.93 \pm 0.31	62.16 \pm 0.18	64.67 \pm 0.31	64.19 \pm 0.24	61.94 \pm 0.40	64.98\pm0.59	64.62 \pm 0.46	63.53 \pm 0.44	64.54 \pm 0.45	57.01 \pm 0.01	65.76\pm0.21
3,800	68.61 \pm 0.44	66.83 \pm 0.25	71.36\pm0.32	70.77 \pm 0.53	68.41 \pm 0.34	71.90\pm0.36	71.30\pm0.36	70.55 \pm 0.25	71.60\pm0.21	61.30 \pm 0.01	71.84\pm0.36
5,000	73.61 \pm 0.23	70.95 \pm 0.23	75.93 \pm 0.21	75.86 \pm 0.27	72.92 \pm 0.36	75.82 \pm 0.31	76.13\pm0.31	75.24 \pm 0.47	75.46 \pm 0.31	64.09 \pm 0.00	76.36\pm0.05
6,200	75.95 \pm 0.18	73.51 \pm 0.30	78.90\pm0.27	77.92 \pm 0.36	77.00 \pm 0.19	78.84\pm0.27	78.37 \pm 0.20	78.54\pm0.26	78.62\pm0.22	65.79 \pm 0.00	78.66\pm0.16
7,400	78.49 \pm 0.14	75.71 \pm 0.35	80.88\pm0.22	80.94\pm0.16	79.39 \pm 0.30	81.19\pm0.15	81.02\pm0.19	81.10\pm0.24	80.76\pm0.29	67.28 \pm 0.01	81.30\pm0.34
CIFAR-10 dataset											
$ \mathbb{L} $	Random	Prob Cover	BADGE	BALD	Coreset	Uncertainty	Entropy	DBAL	Margin	LDM-s	DCoM
200	6.39 \pm 0.19	10.79\pm0.08	6.31 \pm 0.09	3.30 \pm 0.11	6.39 \pm 0.19	2.59 \pm 0.05	2.74 \pm 0.17	2.61 \pm 0.18	5.09 \pm 0.37	-	10.59\pm0.19
400	8.74 \pm 0.07	13.53 \pm 0.22	8.27 \pm 0.14	6.63 \pm 0.23	8.62 \pm 0.17	4.59 \pm 0.23	4.68 \pm 0.23	4.41 \pm 0.30	7.58 \pm 0.17	-	14.11\pm0.11
600	10.73 \pm 0.13	15.86 \pm 0.16	10.29 \pm 0.27	8.33 \pm 0.31	10.39 \pm 0.25	6.52 \pm 0.38	6.32 \pm 0.27	5.94 \pm 0.28	10.20 \pm 0.16	-	16.66\pm0.11
1,000	13.49 \pm 0.18	19.49 \pm 0.20	13.66 \pm 0.26	11.42 \pm 0.26	12.94 \pm 0.21	9.98 \pm 0.38	9.31 \pm 0.22	8.47 \pm 0.35	13.28 \pm 0.19	-	20.21\pm0.07
3,000	24.02 \pm 0.27	29.31 \pm 0.42	24.24 \pm 0.28	22.10 \pm 0.11	23.00 \pm 0.28	21.93 \pm 0.26	20.15 \pm 0.33	20.29 \pm 0.23	23.71 \pm 0.31	-	30.36\pm0.08
5,000	31.52 \pm 0.39	34.64 \pm 0.15	32.18 \pm 0.33	29.58 \pm 0.38	31.41 \pm 0.26	30.60 \pm 0.40	29.15 \pm 0.46	29.60 \pm 0.28	31.66 \pm 0.23	-	36.95\pm0.10
7,000	37.69 \pm 0.16	38.36 \pm 0.13	38.09 \pm 0.10	34.36 \pm 0.20	38.24 \pm 0.16	35.87 \pm 0.19	35.11 \pm 0.11	35.67 \pm 0.35	38.16 \pm 0.17	31.85 \pm 0.00	41.52\pm0.25
11,000	45.66 \pm 0.22	44.69 \pm 0.20	47.00\pm0.16	44.37 \pm 0.28	46.53 \pm 0.18	45.23 \pm 0.20	45.01 \pm 0.17	44.31 \pm 0.24	46.37 \pm 0.36	40.88 \pm 0.01	46.86\pm0.28
15,000	50.57 \pm 0.09	49.58 \pm 0.46	52.42\pm0.17	51.02 \pm 0.09	52.19\pm0.29	51.82 \pm 0.16	51.43 \pm 0.21	51.30 \pm 0.35	52.37\pm0.19	46.59 \pm 0.01	52.33\pm0.22
19,000	54.95 \pm 0.09	52.90 \pm 0.14	56.32 \pm 0.07	55.55 \pm 0.27	56.72\pm0.31	56.55\pm0.21	55.76 \pm 0.31	55.75 \pm 0.14	56.73\pm0.24	49.41 \pm 0.01	56.53\pm0.07
23,000	57.74 \pm 0.14	56.29 \pm 0.21	59.60\pm0.16	59.96\pm0.35	59.59\pm0.22	59.79\pm0.23	59.91\pm0.08	59.72\pm0.21	59.88\pm0.21	52.48 \pm 0.00	59.60\pm0.33
CIFAR-100 dataset											
$ \mathbb{L} $	Random	Prob Cover	BADGE	BALD	Coreset	Uncertainty	Entropy	DBAL	Margin	DCoM	
200	8.25 \pm 0.65	12.33\pm0.34	8.82 \pm 0.18	4.46 \pm 0.31	8.31 \pm 0.52	4.26 \pm 0.26	4.11 \pm 0.09	4.26 \pm 0.24	6.50 \pm 0.94	12.27\pm0.04	
400	12.18 \pm 0.29	16.64 \pm 0.29	12.73 \pm 0.42	9.49 \pm 0.84	9.40 \pm 0.59	7.74 \pm 0.41	7.01 \pm 0.37	6.45 \pm 0.33	11.48 \pm 0.72	18.03\pm0.21	
600	14.85 \pm 0.53	20.38 \pm 0.47	15.69 \pm 0.38	11.21 \pm 0.41	10.68 \pm 0.35	10.38 \pm 0.27	11.28 \pm 0.54	10.34 \pm 0.46	14.74 \pm 0.35	21.77\pm0.62	
1,000	19.71 \pm 0.53	25.76 \pm 0.34	20.91 \pm 0.43	14.85 \pm 0.35	13.47 \pm 0.32	16.30 \pm 0.60	16.52 \pm 0.12	15.10 \pm 0.65	19.47 \pm 0.45	26.88\pm0.00	
3,000	39.06 \pm 0.21	39.98 \pm 0.23	38.51 \pm 0.15	32.40 \pm 0.40	28.80 \pm 0.45	32.52 \pm 0.63	32.97 \pm 0.34	31.60 \pm 0.60	37.00 \pm 0.65	43.40\pm0.29	
5,000	48.33 \pm 0.27	45.08 \pm 0.16	49.47 \pm 0.26	45.04 \pm 0.47	40.10 \pm 0.31	42.05 \pm 0.29	41.65 \pm 0.22	42.41 \pm 0.52	47.24 \pm 0.50	50.76\pm0.08	
7,000	55.12\pm0.09	47.34 \pm 0.44	55.25\pm0.34	53.48 \pm 0.38	49.48 \pm 0.19	51.30 \pm 0.68	49.74 \pm 0.21	49.67 \pm 0.46	54.78\pm0.29	55.17\pm0.34	
11,000	63.46 \pm 0.15	52.79 \pm 0.17	64.68\pm0.15	63.65 \pm 0.32	60.13 \pm 0.11	60.10 \pm 0.50	60.89 \pm 0.34	60.58 \pm 0.25	63.90 \pm 0.22	63.51 \pm 0.31	
15,000	69.42 \pm 0.20	55.04 \pm 0.06	70.27\pm0.25	70.08\pm0.21	67.38 \pm 0.17	67.49 \pm 0.19	66.34 \pm 0.16	66.65 \pm 0.23	69.36 \pm 0.24	70.19\pm0.45	
19,000	72.54 \pm 0.21	62.66 \pm 0.19	73.70\pm0.29	73.63\pm0.21	71.87 \pm 0.14	72.78 \pm 0.41	71.55 \pm 0.27	71.85 \pm 0.17	73.52 \pm 0.23	74.29\pm0.50	
23,000	75.99 \pm 0.16	70.06 \pm 0.27	76.65 \pm 0.11	77.17\pm0.06	75.30 \pm 0.24	76.37 \pm 0.29	75.73 \pm 0.25	75.64 \pm 0.27	77.12\pm0.30	76.68 \pm 0.20	
ImageNet-50 dataset											
$ \mathbb{L} $	Random	Prob Cover	BADGE	BALD	Coreset	Uncertainty	Entropy	DBAL	Margin	DCoM	
200	4.58 \pm 0.13	6.72\pm0.07	4.67 \pm 0.16	1.99 \pm 0.22	4.58 \pm 0.13	2.01 \pm 0.06	1.99 \pm 0.10	1.83 \pm 0.06	1.84 \pm 0.12	6.87\pm0.18	
400	6.61 \pm 0.17	9.30 \pm 0.23	6.42 \pm 0.23	4.39 \pm 0.39	5.53 \pm 0.16	3.50 \pm 0.32	4.17 \pm 0.33	3.65 \pm 0.25	4.71 \pm 0.10	10.59\pm0.26	
600	8.11 \pm 0.42	12.71 \pm 0.42	8.01 \pm 0.20	6.42 \pm 0.24	6.45 \pm 0.37	4.93 \pm 0.29	5.51 \pm 0.33	4.96 \pm 0.22	6.46 \pm 0.12	13.61\pm0.15	
1,000	11.43 \pm 0.17	17.71\pm0.27	11.56 \pm 0.38	9.42 \pm 0.19	9.04 \pm 0.66	7.97 \pm 0.82	8.39 \pm 0.18	7.45 \pm 0.18	10.43 \pm 0.11	17.53\pm0.23	
3,000	27.59 \pm 0.76	34.01 \pm 0.15	27.58 \pm 0.72	24.96 \pm 0.23	19.41 \pm 0.32	23.10 \pm 0.60	20.97 \pm 0.33	20.88 \pm 0.52	26.51 \pm 0.79	34.85\pm0.23	
5,000	39.25 \pm 0.26	41.91 \pm 0.20	39.13 \pm 0.06	36.50 \pm 0.25	29.35 \pm 0.39	33.78 \pm 0.46	31.89 \pm 0.24	31.25 \pm 0.21	38.37 \pm 0.10	44.09\pm0.83	
7,000	46.88 \pm 0.25	48.41 \pm 0.42	46.42 \pm 0.41	43.49 \pm 0.42	38.45 \pm 0.12	42.09 \pm 0.54	41				

$ \mathbb{L} $	Random	Prob Cover	BALD	Coreset	Uncertainty	Entropy	DBAL	Margin	DCoM
400	3.10 \pm 0.07	5.28\pm0.08	1.18 \pm 0.21	3.10 \pm 0.07	1.19 \pm 0.07	1.17 \pm 0.13	1.29 \pm 0.06	2.22 \pm 0.50	5.20\pm0.02
800	4.61 \pm 0.10	7.56 \pm 0.15	2.90 \pm 0.29	3.68 \pm 0.12	2.06 \pm 0.24	2.20 \pm 0.19	2.15 \pm 0.20	3.85 \pm 0.34	8.39\pm0.07
1,200	5.88 \pm 0.25	10.10 \pm 0.08	4.32 \pm 0.33	4.84 \pm 0.14	3.42 \pm 0.19	3.71 \pm 0.26	3.42 \pm 0.16	5.54 \pm 0.23	11.56\pm0.07
2,000	9.51 \pm 0.33	15.25 \pm 0.26	6.73 \pm 0.26	6.78 \pm 0.15	5.72 \pm 0.41	6.15 \pm 0.04	5.72 \pm 0.15	9.17 \pm 0.34	16.27\pm0.08
6,000	25.67 \pm 0.16	32.89\pm0.12	19.85 \pm 0.26	17.98 \pm 0.10	20.12 \pm 0.11	19.89 \pm 0.35	18.72 \pm 0.08	26.03 \pm 0.08	32.76\pm0.13
10,000	37.49 \pm 0.26	42.00\pm0.16	31.36 \pm 0.46	28.31 \pm 0.10	32.13 \pm 0.16	31.57 \pm 0.28	31.00 \pm 0.59	37.33 \pm 0.08	41.97\pm0.44
15,000	46.22 \pm 0.30	48.89 \pm 0.09	41.16 \pm 0.49	38.53 \pm 0.18	42.53 \pm 0.29	41.88 \pm 0.31	41.42 \pm 0.13	46.37 \pm 0.17	49.47\pm0.27
20,000	52.20 \pm 0.19	51.70 \pm 0.32	48.79 \pm 0.58	46.59 \pm 0.15	49.50 \pm 0.25	48.07 \pm 0.36	47.89 \pm 0.13	53.01 \pm 0.19	54.25\pm0.26
40,000	64.57 \pm 0.17	57.60 \pm 0.05	64.02 \pm 0.37	61.78 \pm 0.30	63.94 \pm 0.27	63.14 \pm 0.37	63.21 \pm 0.13	65.19 \pm 0.24	65.69\pm0.17

ImageNet-200 dataset

$ \mathbb{L} $	Random	Prob Cover	BADGE	BALD	Coreset	Uncertainty	Entropy	DBAL	Margin	DCoM
10	15.73\pm0.90	17.26\pm0.78	14.92 \pm 0.98	12.22 \pm 0.91	15.58\pm1.03	11.88 \pm 0.83	11.67 \pm 0.48	11.79 \pm 1.06	12.81 \pm 0.65	16.72\pm0.94
20	16.68 \pm 0.77	22.81\pm0.28	18.24 \pm 0.46	15.28 \pm 0.98	18.25 \pm 0.97	16.05 \pm 0.94	18.48 \pm 0.67	18.19 \pm 0.63	15.65 \pm 1.35	23.47\pm0.75
30	19.78 \pm 0.79	24.91 \pm 0.49	19.80 \pm 0.38	18.37 \pm 1.06	19.41 \pm 0.92	17.75 \pm 1.05	19.33 \pm 0.74	20.35 \pm 0.90	18.49 \pm 1.16	26.72\pm0.79
40	21.49 \pm 0.48	26.56 \pm 0.48	21.57 \pm 0.48	21.25 \pm 0.95	20.45 \pm 1.00	20.86 \pm 0.77	21.45 \pm 0.74	21.70 \pm 0.88	20.97 \pm 0.71	28.58\pm0.69
50	22.19 \pm 0.33	28.30\pm0.42	24.40 \pm 0.45	22.13 \pm 0.56	21.76 \pm 1.07	22.11 \pm 0.81	22.75 \pm 0.60	22.76 \pm 0.91	23.57 \pm 0.59	29.20\pm0.87
200	36.04 \pm 0.59	40.91 \pm 0.33	35.50 \pm 0.57	32.89 \pm 0.50	33.22 \pm 0.55	33.44 \pm 0.76	34.38 \pm 0.58	34.95 \pm 0.46	36.05 \pm 0.53	41.74\pm0.49
400	44.07 \pm 0.60	49.52\pm0.23	44.18 \pm 0.54	43.33 \pm 0.45	41.83 \pm 0.39	42.39 \pm 0.64	42.51 \pm 0.46	43.67 \pm 0.47	44.35 \pm 0.52	47.02 \pm 0.73
600	50.02 \pm 0.44	52.65\pm0.35	50.10 \pm 0.44	49.56 \pm 0.32	48.91 \pm 0.32	49.46 \pm 0.48	48.85 \pm 0.38	49.23 \pm 0.49	49.27 \pm 0.59	51.54\pm0.86
800	53.69 \pm 0.36	54.45\pm0.56	54.57\pm0.63	54.20\pm0.51	54.42\pm0.21	53.48 \pm 0.38	53.70 \pm 0.38	53.98 \pm 0.31	54.05\pm0.56	55.05\pm0.71
1,400	62.00 \pm 0.26	61.54 \pm 0.30	63.38\pm0.25	62.82\pm0.51	62.72\pm0.42	62.42 \pm 0.27	62.24 \pm 0.23	63.04\pm0.23	63.11\pm0.25	63.04\pm0.57
2,600	70.18 \pm 0.27	70.50 \pm 0.08	72.76\pm0.19	72.72\pm0.26	71.41 \pm 0.13	72.53 \pm 0.23	72.35 \pm 0.18	72.97\pm0.18	72.12 \pm 0.40	72.93\pm0.33
3,800	75.51 \pm 0.21	72.97 \pm 0.17	76.75\pm0.15	76.69 \pm 0.11	75.75 \pm 0.09	76.80\pm0.21	77.05\pm0.15	76.85\pm0.09	76.91\pm0.10	76.92\pm0.18

STL-10 dataset

$ \mathbb{L} $	Random	Prob Cover	BADGE	BALD	Coreset	Uncertainty	Entropy	DBAL	Margin	LDM-s	DCoM
10	11.36 \pm 0.50	11.80 \pm 0.08	13.26\pm0.79	13.84\pm1.64	11.36 \pm 0.50	11.41\pm0.85	11.06\pm1.38	11.66\pm0.56	10.80 \pm 0.66	-	12.62\pm0.60
20	11.05 \pm 0.41	10.96 \pm 0.19	12.19 \pm 0.67	12.74 \pm 1.26	10.99 \pm 0.59	11.81 \pm 0.84	10.86 \pm 0.58	14.94\pm0.36	12.50 \pm 0.95	-	13.30 \pm 0.26
30	11.16 \pm 0.36	12.19\pm0.52	12.12\pm0.51	14.22\pm2.01	11.10 \pm 0.29	12.66\pm1.28	11.86\pm0.65	13.50\pm0.46	11.56\pm0.79	-	13.91\pm0.32
40	11.85 \pm 0.46	12.11 \pm 0.20	12.71 \pm 0.70	13.98\pm2.06	11.57 \pm 0.57	14.16\pm1.63	12.28 \pm 0.47	13.10 \pm 0.41	11.76 \pm 0.75	-	14.32\pm0.14
50	12.55 \pm 0.49	12.86 \pm 0.36	12.47 \pm 0.89	13.18\pm2.00	11.76 \pm 0.38	14.12\pm1.00	12.72 \pm 0.54	12.88 \pm 0.54	12.04 \pm 0.68	-	15.09\pm0.25
200	22.32 \pm 0.84	24.34\pm0.44	20.18 \pm 1.09	19.00 \pm 1.66	17.42 \pm 1.03	21.99 \pm 1.11	20.38 \pm 1.08	20.98 \pm 0.99	22.03 \pm 0.87	-	24.58\pm1.10
400	36.24 \pm 1.24	40.42 \pm 0.67	35.13 \pm 0.40	28.74 \pm 2.78	28.88 \pm 1.47	29.58 \pm 0.55	33.01 \pm 1.36	33.06 \pm 1.82	34.01 \pm 0.18	-	46.90\pm1.56
600	47.29 \pm 0.98	52.67 \pm 0.75	46.46 \pm 0.87	37.26 \pm 1.56	40.24 \pm 1.24	42.65 \pm 0.68	42.89 \pm 1.38	43.99 \pm 0.46	46.69 \pm 0.50	-	58.34\pm1.25
800	56.32 \pm 0.50	62.96 \pm 0.51	56.48 \pm 1.33	47.47 \pm 2.46	49.74 \pm 1.42	50.62 \pm 2.03	53.17 \pm 1.64	46.45 \pm 1.14	55.27 \pm 1.05	-	65.90\pm0.97
1,400	74.00 \pm 0.38	73.16 \pm 0.21	75.53 \pm 0.77	65.33 \pm 3.30	68.44 \pm 0.69	72.13 \pm 0.98	72.81 \pm 1.09	73.14 \pm 0.69	74.53 \pm 0.74	79.02\pm0.01	78.36 \pm 0.36
2,600	83.24 \pm 0.48	81.94 \pm 0.08	86.56\pm0.24	83.33 \pm 0.96	83.83 \pm 0.39	85.80 \pm 0.31	84.72 \pm 0.54	84.83 \pm 0.59	86.33\pm0.13	83.76 \pm 0.00	86.31\pm0.26
3,800	87.18 \pm 0.14	85.34 \pm 0.11	89.61\pm0.25	88.91 \pm 0.54	88.86 \pm 0.14	89.64\pm0.09	88.79 \pm 0.14	89.36 \pm 0.15	89.34 \pm 0.18	86.08 \pm 0.00	89.28 \pm 0.13
5,000	88.79 \pm 0.15	87.58 \pm 0.20	91.72\pm0.15	90.93 \pm 0.14	91.24 \pm 0.17	91.55\pm0.04	91.13 \pm 0.11	91.28 \pm 0.12	91.75\pm0.17	87.58 \pm 0.00	91.50\pm0.08
6,200	90.16 \pm 0.04	88.55 \pm 0.10	92.64\pm0.09	92.46 \pm 0.04	92.35 \pm 0.03	92.63\pm0.08	92.56\pm0.16	92.65\pm0.10	92.55\pm0.12	88.64 \pm 0.00	92.54\pm0.12
7,400	90.99 \pm 0.11	89.71 \pm 0.08	93.56\pm0.05	93.26 \pm 0.10	93.02 \pm 0.14	93.33 \pm 0.05	93.38 \pm 0.11	93.43\pm0.13	89.56 \pm 0.00	93.47\pm0.09	

SVHN dataset

Table 4: Model accuracy for different sizes of labeled set \mathbb{L} and AL strategies.

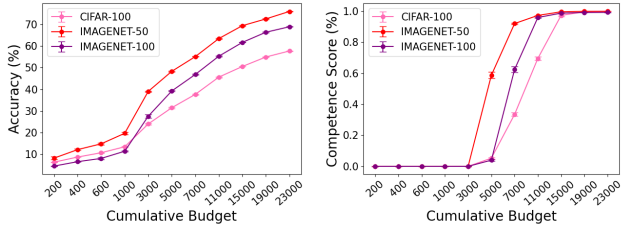
measured by accuracy. Interestingly, while the critical point where $S_{\mathcal{L}}$ changes from favoring \mathcal{O}_{low} (small values) to favoring \mathcal{O}_{high} (large values) corresponds to an intermediate level of accuracy, this transition is delayed for the more difficult datasets.

E.4 Different embedding space

In Section 4.3, we present an ablation study where we repeat the basic fully-supervised experiments while varying the embedding employed by *DCoM*. In Fig. 12 you can see the same ablation using BYOL (Grill et al. 2020) representation.

E.5 Comparison per dataset

Tables 3-4 present the empirical accuracy values of several datasets using different active learning algorithms. In each active step, a new learner is trained from scratch over all available labeled data, and the results are presented as the [mean \pm STE] over 5 – 10 repetitions (3 for ImageNet subsets). As mentioned earlier, the results for LDM-s algorithm were acquired from the study by (Cho et al. 2023). Their lack of code provision suggests discrepancies in the running setup. Nonetheless, the disparity between their method and random selection in their setup is smaller than that observed in ours, implying the superiority of our method. The table



(a) Accuracy with random sampling. (b) $S_{\mathcal{L}}$ during $DCoM$ training.

Figure 11: (a) Accuracy (mean and standard error) as a function of budget b , learning to classify CIFAR-100, ImageNet-50, and ImageNet-100 using a random sample of b points. (b) The competence score $S_{\mathcal{L}}$ as a function of budget.

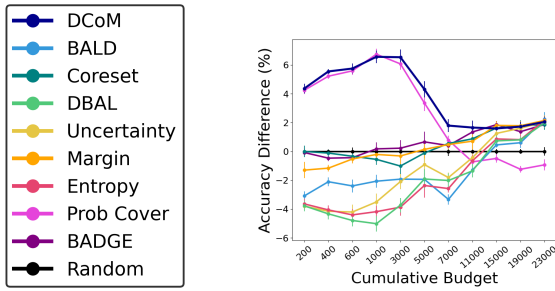


Figure 12: Performance over CIFAR-100, using BYOL feature space over $DCoM$ and $ProbCover$, see details in the caption of Fig. 3. Clearly, $DCoM$ consistently achieves the best results.

includes the results for all datasets, with the name of each dataset below it.